Natural Hazards
and Earth System
Sciences

Towards a global impact-based forecasting model for tropical cyclones

Mersedeh Kooshki Forooshani[1]**, Marc van den Homberg**[2]**, Kyriaki Kalimeri**[1]**, Andreas Kaltenbrunner**[1,4]**,**
Yelena Mejova[1]**, Leonardo Milano**[3]**, Pauline Ndirangu**[3]**, Daniela Paolotti**[1]**, Aklilu Teklesadik**[2]**, and Monica L. Turner**[3]

[1]ISI Foundation, Turin, Italy
[2]510, an Initiative of the Netherlands Red Cross, the Hague, the Netherlands
[3]UN OCHA Centre for Humanitarian Data, the Hague, the Netherlands
[4]Internet Interdisciplinary Institute, Universitat Oberta de Catalunya, Barcelona, Spain

Correspondence: Marc van den Homberg (mvandenhomberg@redcross.nl) and Andreas Kaltenbrunner
(kaltenbrunner@gmail.com)

Abstract. Tropical cyclones (TCs) produce strong winds
and heavy rains accompanied by consecutive events such
as landslides and storm surges, resulting in losses of lives
and livelihoods, particularly in regions with high socioeco-
nomic vulnerability. To proactively mitigate the impacts of
TCs, humanitarian actors implement anticipatory action. In
this work, we build upon such an existing anticipatory ac-
tion for the Philippines, which uses an impact-based fore-
casting model for housing damage based on eXtreme Gradi-
ent Boosting (XGBoost) to release funding and trigger early
action. We improve it in three ways. First, we perform a cor-
relation and selection analysis to understand if Philippines-
specific features can be left out or replaced with features from
open global data sources. Secondly, we transform the target
variable (percentage of completely damaged houses) and not
yet grid-based global features to a 0.1° grid resolution by de-
aggregation using Google Open Buildings data. Thirdly, we
evaluate XGBoost regression models using different combi-
nations of global and local features at grid and municipality
spatial levels. We first introduce a two-stage model to pre-
dict if the damage is above 10 % and then use a regression
model trained on all or only high-damage data. All experi-
ments use data from 39 typhoons that impacted the Philip-
pines between 2006–2020. Due to the scarcity and skewness
of the training data, specific attention is paid to data strat-
ification, sampling, and validation techniques. We demon-
strate that employing only the global features does not sig-
nificantly influence model performance. Despite excluding

local data on physical vulnerability and storm surge suscepti-
bility, the two-stage model improves upon the municipality-
based model with local features. When applied to anticipa-
tory action, our two-stage model would show a higher true-
positive rate, a lower false-negative rate, and an improved
false-positive rate, implying that fewer resources would be
wasted in anticipatory action. We conclude that relying on
globally available data sources and working at the grid level
holds the potential to render a machine-learning-based im-
pact model generalizable and transferable to locations out-
side of the Philippines impacted by TCs. Also, a grid-based
model increases the resolution of the predictions, which may
allow for a more targeted implementation of anticipatory ac-
tion. However, it should be noted that an impact-based fore-
casting model can only be as good as the forecast skill of
the TC forecast that goes into it. Future research will focus
on replicating and testing the approach in other TC-prone
countries. Ultimately, a transferable model will facilitate the
scaling up of anticipatory action for TCs.

1 Introduction

The emission of greenhouse gases due to human activity in
the past decades has had a significant effect on global climate
variability, and the resulting climate change will likely in-
crease conditions that shape extreme events such as tropical
cyclones (TCs) (Van Aalst, 2006). TCs are massive storms

that form over warm tropical oceans and cause extreme rainfall (Navarro and Merino, 2022), also leading to consecutive events such as landslides (Jones et al., 2023), storm surges (Bloemendaal et al., 2019), and floods (Eilander et al., 2022). Over 20 million people have been affected by TCs, and almost USD 30 billion in damages have been reported yearly in the last 2 decades (Geiger et al., 2018). For 2022, the Emergency Events Database (EM-DAT, 2022) reports that 36.9 million people were affected by storms, and these storms were responsible for USD 90.2 billion of economic loss. TCs occur in many parts of the world but mainly in North America, East Asia, and the Caribbean–Central American region (Gettelman et al., 2018; Mendelsohn et al., 2012). Significantly, the population and infrastructure close to the coast (Rogers et al., 2019) get impacted by TCs. Developing countries are disproportionately affected, as their population is and will – with climate change – be more exposed (Bloemendaal et al., 2022) and more vulnerable to TCs due to their socioeconomic conditions (Hallegatte et al., 2016).

Until recently, humanitarian action has been primarily reactive, only initiating a response after a disaster. However, over the past decade, the increased amount of data availability and improved weather forecasting capability have enabled humanitarian actors to implement anticipatory action (AA), focusing on reducing the impacts of a hazard before it occurs (van den Homberg et al., 2020). AA plays a crucial role in enabling humanitarian organizations to mitigate the impact of various shocks proactively, and recent evidence suggests that AA is more dignified, swift, and cost-effective than humanitarian response (Chaves-Gonzalez et al., 2022).

AA triggers are built using hazard- or impact-based forecasts (Harrison et al., 2022). If the forecast exceeds a predetermined threshold (with a certain probability), early actions are implemented to save lives and protect property and livelihoods (Yonson et al., 2018). Around the world, many governmental and humanitarian actors are working hand in hand to develop AA mechanisms (Anticipation Hub, 2022). The Red Cross and Red Crescent National Societies of seven countries have implemented AA for TCs with a large group of in-country stakeholders, i.e., Bangladesh, Mozambique, the Philippines, Costa Rica, Guatemala, Honduras, and Madagascar. Similarly, the United Nations Office for the Coordination of Humanitarian Affairs (OCHA) has piloted AA in multiple countries for several hazards, particularly TCs, together with the Philippine Red Cross (ReliefWeb, 2022).

Among the many countries at risk of TCs, the WorldRiskReport 2022 (https://weltrisikobericht.de/en/, last access: 15 September 2023) put the Philippines at the number one spot for the most disaster-prone country in the world (Atwii et al., 2022). The Philippines is recognized as a global "hot spot" for natural hazards and endures a higher frequency of disasters due to earthquakes, typhoons, floods, and landslides than any other country, with an average of eight or nine disasters annually (Santos, 2021). After reviewing TC data from 1951 to 2013 in the Philippines, it was found that

the Philippine Area of Responsibility experiences an average of nearly 20 TCs every year (Cinco et al., 2016).

In 2016, the 510 initiative of the Netherlands Red Cross started working with the Philippine and German Red Cross to develop a model to predict the humanitarian impact of typhoons. Initially, the emphasis was on understanding the needs of the humanitarian decision-makers and collecting and collating data on several features and target values of the model through desk research and in-country visits of key stakeholders (Van Lint et al., 2016). Since the first model in 2016, this model, which, for simplicity, we will refer to in the remainder of the paper as the 510 model, has undergone many iterations to improve its performance further. In 2019, the 510 model (Teklesadik et al., 2023; Teklesadik and van den Homberg, 2022) was approved as the trigger model for the early action protocol for typhoons (https://reliefweb.int/report/philippines/philippines-typhoon-early-action-protocol-summary-november-2019, last access: 15 September 2023) and in 2021 as the trigger model for the UN OCHA AA pilot. This approach combines historical impact and vulnerability data with typhoon tracks and weather forecasts to generate early estimates of the expected damage of a typhoon before landfall. The model was specifically built for the Philippines.

In this study, we pursue two goals. First, due to the global prevalence of TCs and their disproportional impact on developing countries, we aim to extend the 510 model to other geographical contexts to create a globally applicable impact model for TCs. For this purpose, we select features that we can use for different geographical contexts (i.e., countries) because the data for these features can be selected from open-access global databases. Secondly, we seek to ensure the model's performance is not deteriorated in this process and, if possible, improved.

The 510 model is a probabilistic typhoon impact prediction model whose spatial configuration is vector-based where model inputs are aggregated per municipality (Teklesadik et al., 2023; Teklesadik and van den Homberg, 2022). This approach was chosen due to the usage of localized datasets collected at the municipality level. However, there are two reasons why a grid-based model configuration should be a better approach to test the hypothesis of porting the typhoon model to other contexts: firstly, because open datasets, for example, for hazard, exposure, and vulnerability, are often grid-based and, secondly, because such models become independent of the specific geographic resolution of administrative regions in a given territory. To test this hypothesis, we assess the performance of a variant of the 510 model still in the context of the Philippines but only using globally available variables. We then implement a model with grid-based spatial configuration using only the globally available features. To compare the performance of this grid-based model with the 510 model, we transform its prediction results back to the municipality level. Finally, to achieve better performance of the grid-based model, we include additional globally avail-

able features that were not used in the 510 model and build a novel two-step prediction model. We illustrate the capacity of this new approach concerning correctly predicting damage levels above a given threshold, which would trigger early actions. Our results allow us to conjecture about the feasibility of generalizing our particular grid-based model to other countries and reducing the impact of humanitarian crises, with the ultimate goal of saving lives and protecting livelihoods from disasters due to TCs.

2 Related literature

Disasters manifest in various regions globally, driven by a confluence of hazard occurrence, exposure levels, and the vulnerability of human populations and valuable assets. Historically, national meteorological and hydrological services (NMHSs) only focused on furnishing weather-related information and warnings based on meteorological factors such as wind speeds, rainfall, and hazard location and timing. Nevertheless, in the past decade, NMHSs and their collaborating agencies have made substantial efforts to enhance their comprehension of the potential repercussions of severe hazards. Achieving this goal necessitates robust partnerships with collaborating agencies and extensive research into impact-based forecasting models, incorporating exposure and vulnerability data.

Early studies assessed the impacts of floods and TCs in different aspects. In one of these first studies by Vickery et al. (2006), a hurricane model named HAZUS-MH was developed to predict the building damage caused by hurricanes in the USA. This model has been validated using damage data collected during post-storm damage surveys and insurance loss. Later, in a study by Liu et al. (2009), historical data of typhoon disasters in China were used to prevent and mitigate the life and property losses due to these phenomena in New Orleans and Shanghai. The study found a stronger correlation between wind speed and water level than other variables.

Another early study about coastal flood risks was done by Boettle et al. (2011) and was based on estimating typical damages caused by storm surges. This study determined that although the damage depends on various factors, such as flow velocity and flood duration, the correlation between flood occurrences and the average damages is typically explained using a stage–damage function, which employs the maximum water level as the only damage influencing factor.

In a study by Wagenaar et al. (2018), a flood damage model was proposed, using random forest (RF) and Bayesian network (BN) approaches to estimate the residential damage based on water depth and average building value. The study leveraged data from Germany and the Netherlands to cross-validate the model performances. Alternatively, Kim et al. (2019) used regression models to determine whether typhoon damage is correlated with wind speed, rainfall, and the number of cutting slopes and then assess the impact of built environment vulnerability on financial loss using typhoon data. More recently, a hybrid model using convolutional neural networks (CNNs) and long short-term memory (LSTM) was introduced by Chen et al. (2019) as a predictive model of western North Pacific typhoon formation and intensity with an emphasis on the various spatial and temporal features of typhoons.

In 2020, a statistical prediction model was proposed by Kim et al. (2020) for China. Its data included daily rainfall data for 55 typhoons between 1961 and 2017 from 537 meteorological stations in China. The model was based on the principle of track similarity and used different methods, such as fuzzy C-means (FCM) clustering and intensity correction. This model aimed to improve the typhoon-induced accumulated rainfall forecasts over China. In another recent study, a group of researchers (Hou et al., 2020) built a hybrid model to predict the damage probability of transmission lines under each wind field for a particular typhoon named Mangkhut (2018; Mangkhut18, with storms labeled with their name and a two-digit year throughout the paper) in China. It used the Monte Carlo method to simulate the random wind field to improve the prediction with RF.

For the specific context of the Philippines as one of the most climate-disaster-prone countries, some research has been done in the past few years. Recently, Wagenaar et al. (2021) made notable contributions by proposing models based on RF and artificial neural network (ANN) approaches. They used data from 12 typhoons in the Philippines at the municipality level to explain the relationships between damage and the variables that can explain damage, such as water depth or wind speed. The Red Cross collected this dataset, including 40 variables from which damage is predicted. In another recent study, Lambert et al. (2022) utilized the following machine learning (ML) algorithms: RF, k-nearest neighbor (KNN), and generalized linear models (GLMs) to predict the damage caused by urban forest storms. They reported that GLM and RF models gave overall unbiased damage predictions across all methods and rarity levels, while KNN consistently underpredicted damage. A vulnerability risk model for the Philippines was put forward by Baldwin et al. (2023), in which they assess the vulnerability using the wind field data and total asset value and determine the expected asset loss. In a study, Walsh (2020) proposed a traditional expanded risk assessment using asset losses as the primary metric to measure the severity of a disaster.

Finally, the already mentioned 510 model (Teklesadik et al., 2023) was developed recently by the Netherlands Red Cross as a vector-based or municipality-based prediction model to estimate the damage to houses caused by TCs in the Philippines. It used data from 39 typhoons with mild to severe damage impact, and the independent variables included 36 features related to hazard characteristics and vulnerability data, all at the municipality level. In this study, we aim to expand the applicability of this model to other contexts by

constraining its feature set to internationally available data while improving its performance in the Philippines setting.

3 Data and methodology

This study is based on data and features employed by Teklesadik and van den Homberg (2022) in the 510 model (see also Teklesadik et al., 2023) to train a typhoon-impact-based forecasting model. It includes data from 39 typhoons that impacted the Philippines between 2006 and 2020 collected from various organizations and resources and at different spatial resolutions. For example, data on damaged houses are collected at the individual housing level but only available in an open-access format at an aggregated municipality level (i.e., admin level 3 in the Philippines). We extend this model by using additional data (available on a global scale) and improve the prediction and evaluation methods. Table 1 shows the features used in previous work (the 510 model), the ones added in this study, and their descriptions. Note that the model used by Teklesadik et al. (2023) operated at the municipality level, while the models we developed use data in a 0.1° grid format[1] whose area is smaller than the average size of a municipality. There are 3726 cells in our data that overlap with land. Although most of the features in our developed grid-based models are directly available at the 0.1° resolution, some are transformed to grid resolution after being obtained from their sources at the municipality level. Below, we describe the features, the target variable, and the transformation process (when applicable) in more detail.

3.1 Target variable

The target variable of the models analyzed in this study is the percentage of fully damaged houses at the municipality level. The Department of Social Welfare and Development collects these data at the individual house level, assigning a partially or fully damaged[2] label to each house (DSWD Central Office, 2019). A house is a dwelling or structure used for human habitation, especially by a family or small group. Based on this damage label, people are eligible for emergency shelter assistance. The data are only available in an open-access format at the aggregated level of the municipality. We use the percentage of houses fully damaged and unfit for habitation or without any remaining structural features. This damage variable can vary in the range between 0 % and 100 %.

Housing damage is improbable to occur under below-average rainfall and wind speed conditions. Hence, missing damage percentage values in the original data of the municipality-based 510 model were replaced with 0 for

---

[1]This corresponds to approx. $11 \times 11\,\mathrm{km}^2$. This spatial resolution could be increased for other contexts.

[2]The exact definition of the extent of damage is subject to interpretation of the assessors and the municipality. We assume that this definition does not vary between municipalities.
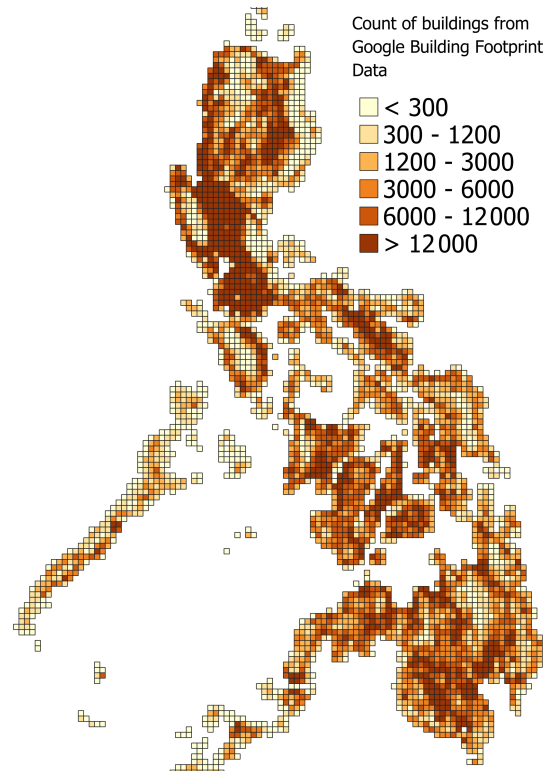

Figure 1. The number of the building centroids from the Google Open Buildings dataset aggregated to a 0.1° grid. The lighter shades of brown indicate grids with fewer buildings, while the darker shades point to grids with more buildings.

records with low wind speed (below $25\,\mathrm{m\,s^{-1}}$) and rainfall (below 50 mm). This choice is also in line with the choice of Bloemendaal et al. (2020), where they stored for each synthetic TC only data when the maximum 10 m 10 min average sustained wind speed was larger than $20\,\mathrm{m\,s^{-1}}$. In contrast, the remaining entries with missing damage values that did not fulfill these conditions have been removed from the dataset. It should be noted that these thresholds are defined based on long-term average observation of climate data.

To improve the resolution of the original 510 model, we transform the original values of damage data from the municipality level to the grid format. To do so, we use the number of buildings from Google Open Buildings data (https://sites.research.google/open-buildings/#download, last access: 15 September 2023) (see Fig. 1 for a visualization of these data) to compute transformation weights. We also checked Microsoft Building Footprints and Open Street Map (OSM) building delineation data, but these datasets were incomplete for the Philippines. Specifically, for a given municipality, we count the number of buildings in each grid cell with a geographical intersection with the municipality and then normalize the data by the number of buildings in a municipality. In this way, we give more weight to the grid cells in which a municipality has more buildings.

Table 1. Description of features employed by the different models. Features 1–36 are used as municipality- and grid-level resolution, while features 37–42 are only used as grid-level resolution. For better comprehension, the labels of some features may differ concerning their original labels in the input data. DSWD: Department of Social Welfare and Development.

No.	Feature label	Description	Local	Global	Global+
1	HAZ_rainfall_Total	Total volume of rain during a typhoon event	✓	x	x
2	HAZ_rainfall_max_6h	Maximum rainfall within a 6 h period (mm)	✓	✓	✓
3	HAZ_rainfall_max_24h	Maximum rainfall within a 24 h period (mm)	✓	✓	✓
4	HAZ_v_max	Max 1 min sustained wind speed, based on wind field (m s^{-1})	✓	✓	✓
5	HAZ_v_max_3	Max 1 min sustained wind speed cubed, based on wind field (m s^{-1})	✓	x	x
6	HAZ_dis_track_min	Minimum distance between typhoon track and municipality	✓	✓	✓
7	HAZ_SEC_landslide_per	Percentage of houses (OSM footprint) in landslide risk zones (red, yellow, orange)	✓	x	x
8	HAZ_SEC_stormsurge_per	Percentage of houses (OSM footprint) in storm surge risk zones (red, yellow, orange)	✓	x	x
9	HAZ_SEC_Bu_p_inSSA	Fraction of municipality colored blue in storm surge risk map	x	x	x
10	HAZ_SEC_Bu_p_LS	Fraction of municipality colored blue in landslide risk map	x	x	x
11	HAZ_SEC_Red_per_LSbldg	Fraction of municipality colored red in landslide risk map	✓	x	x
12	HAZ_SEC_Or_per_LSbldg	Fraction of municipality colored orange in landslide risk map	✓	x	x
13	HAZ_SEC_Yel_per_LSSAb	Fraction of municipality colored yellow in storm surge risk map	✓	x	x
14	HAZ_SEC_Red_per_SSAbldg	Fraction of municipality colored red in storm surge risk map	x	x	x
15	HAZ_SEC_Or_per_SSAbldg	Fraction of municipality colored orange in storm surge risk map	✓	x	x
16	HAZ_SEC_Yellow_per_LSbl	Fraction of municipality colored yellow in storm surge risk map	✓	x	x
17	TOP_mean_slope	Slope mean	✓	✓	✓
18	TOP_mean_elevation_m	Elevation mean	✓	✓	✓
19	TOP_ruggedness_stdev	Ruggedness standard deviation	✓	✓	✓
20	TOP_mean_ruggedness	Ruggedness mean	x	✓	✓
21	TOP_slope_stdev	Slope standard deviation	x	✓	✓
22	TOP_with_coast	Boolean: coast or no coast	✓	✓	✓
23	TOP_coast_length	Length of coast	✓	✓	✓
24	VUL_poverty_perc	Percentage of people in poverty	✓	x	x
25	VUL_Housing_Units	Total number of housing units	✓	✓	✓
26	VUL_StrongRoof_StrongWall	Number of houses with a strong roof and strong walls	✓	x	x
27	VUL_StrongRoof_LightWall	Number of houses with a strong roof and light walls	✓	x	x
28	VUL_StrongRoof_SalvageWall	Number of houses with a strong roof and salvaged walls	✓	x	x
29	VUL_LightRoof_StrongWall	Number of houses with a light roof and strong walls	✓	x	x
30	VUL_LightRoof_LightWall	Number of houses with a light roof and light walls	✓	x	x
31	VUL_LightRoof_SalvageWall	Number of houses with a light roof and salvaged walls	✓	x	x
32	VUL_SalvagedRoof_StrongWall	Number of houses with a salvaged roof and strong walls	✓	x	x
33	VUL_SalvagedRoof_LightWall	Number of houses with a salvaged roof and light walls	✓	x	x
34	VUL_SalvagedRoof_SalvageWall	Number of houses with a salvaged roof and salvaged walls	✓	x	x
35	VUL_vulnerable_groups	Vulnerable groups from DSWD National Household Targeting Office	✓	x	x
36	VUL_pantawid_pamilya_beneficiary	Number of Pantawid Pamilya beneficiary households	✓	x	x
37	VUL_relative_wealth_index (rwi)	Relative standard of living within countries	x	x	✓
38	total_pop	Total population	x	x	✓
39	urban	Proportion of urban areas	x	x	✓
40	rural	Proportion of rural areas	x	x	✓
41	water	Proportion of areas classified as water	x	x	✓
42	Percent_houses_damaged_5years	Percentage of damaged houses in last 5 years	x	x	✓

For the evaluation, which is done at the municipality level, we perform the opposite transformation: we normalize the data by the number of buildings in a grid cell to get the back-transformation weights from grid cells to municipalities. Note that these transformations are not bijections, in the sense that, for example, in a grid cell where only one of its intersecting municipalities has damage larger than 0, during re-aggregation, this damage score will be distributed among the neighboring municipalities intersecting with the grid cell.

Figure 2 shows the distributions of both the original damage variable used by the 510 model (blue) and the re-aggregated (red) damage variables for all typhoons. Note that, after the transformation back from the grid, we gain more data points in the lowest-damage area due to the redistribution of damage data to neighboring municipalities – a property that affects evaluation metrics (as will be discussed in the Results section). Furthermore, as the distribution is heavily skewed (see left panel), we bin the data in the following intervals: [0, 0.00009], (0.00009, 1], (1, 10], (10, 50], and (50,100]. We use these bins for stratification during model training and to compute performance metrics for each bin separately.
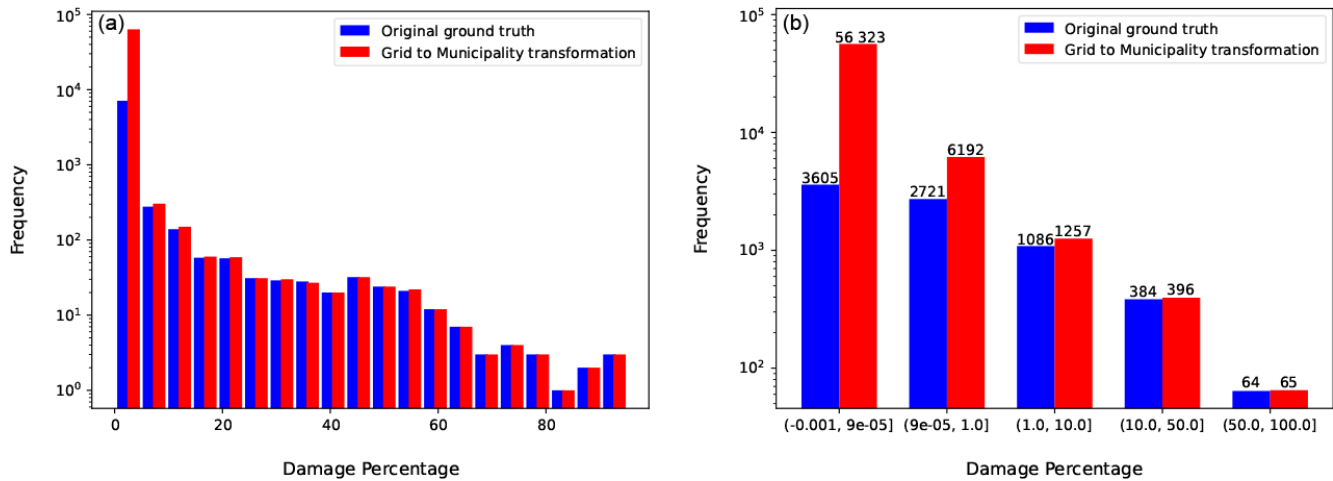
Figure 2. (a) Distribution of damage percentage at the municipality level. **(b)** Stratification by unequally sized bins used for training.
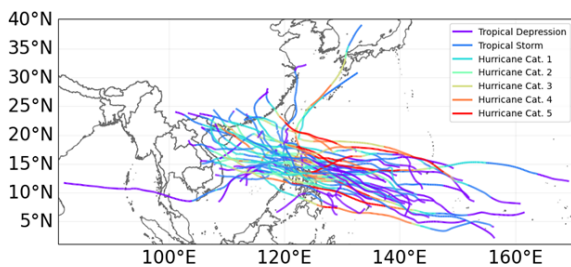

Figure 3. Tropical cyclones (TCs) track data for the Philippine Area of Responsibility with the colors indicating the TC intensity. Categories 1 to 5 refer to the weakest and the strongest, respectively, according to the Saffir–Simpson hurricane wind scale (SSHWS) (Taylor et al., 2010). The naming protocols for TCs vary by region. The term "typhoon" is mostly used in the western North Pacific region, which includes the Philippines. The International Best Track Archive for Climate Stewardship (IBTrACS) data use the hurricane label to refer to a typhoon, regardless of the TC region.

3.2 Original features of the municipality-based model

In this section, we describe those features used in the original 510 model of Teklesadik et al. (2023). As input data for our models, we use both municipality- and grid-based versions of these features. We will indicate this by adding M (for municipality) or G (for grid) as prefixes to the model names. Rows 1 to 36 of Table 1 briefly describe those features, which we extend below. Furthermore, the table also indicates different groups of features in the three rightmost columns, which we label Local, Global, and Global+. They are used in the suffixes of the model names to indicate which subset of features the model uses. We note that the source data for those features used in the Local, Global, and Global+ models are the same, so the Local model has features for which the source data were at the grid level.

1. Features 1–6, with the prefix HAZ, are created from historical typhoon and weather metadata. The source of these features was at the grid level except for the typhoon track data (no. 6 HAZ_dis_track_min), which were directly obtained at the municipality level. Rainfall is obtained from the NASA Precipitation Processing System (PPS), which aggregates weather data from the Global Precipitation Measurement (GPM) project (https://arthurhou.pps.eosdis.nasa.gov/, last access: 15 September 2023). In particular, we use the maximum of the corresponding 6 or 24 h rolling average windows of the 30 min GPM rainfall data. At the same time, the HAZ_rainfall_Total is the sum over all rainfall in a ~ 3 d period of typhoon landfall.

   The typhoon track data were collected from the International Best Track Archive for Climate Stewardship (IBTrACS) (https://www.ncei.noaa.gov/products/international-best-track-archive, last access: 15 September 2023). See Fig. 3 for a visualization of the tracks of the typhoons used in this study. We see a great variety of the spatial distribution of typhoons as they impact different regions of the Philippines.

   The maximum wind speed per municipality was estimated by generating wind fields using CLIMADA (https://wcr.ethz.ch/research/climada.html, last access: 15 September 2023) and the default Holland (2008) model with the B parameter from Holland (1980), which determines the shape of the wind profile (Holland, 1980, 2008).

2. Features 7–16 with the prefix HAZ_SEC are data for landslide- and storm-surge-vulnerable areas. The source of these features was at the grid level. Hazard maps were taken from the National Operational Assessment of Hazards (NOAH) (https://noah.up.edu.ph/, last access: 15 September 2023), and the fraction of each risk

level (set by color) intersecting with each municipality was used to create the features. Unfortunately, these maps are no longer available online.

3. Features 17–23 with the prefix TOP are the topography data, including features related to the slope, terrain ruggedness, elevation, and coastline length. The source data of these features were available at the grid level except for the coastline features (no. 22 TOP_with_coast and no. 23 TOP_coast_length). These were collected via geographic information system (GIS) analysis combined with the Common Operational Datasets for the Philippines (https://cod.unocha.org/, last access: 15 September 2023). All but coastline length were generated using 90 m Shuttle Radar Topography Mission digital elevation model (SRTM DEM) from the Consultative Group on International Agricultural Research Consortium for Spatial Information (CGIAR-CSI) (https://srtm.csi.cgiar.org/, last access: 15 September 2023). Figure 4 shows the corresponding elevation data; Fig. 5 shows the slope data derived from the elevation data; and, finally, Fig. 6 shows the mean slopes aggregated by grid cells. The coastline length was computed from the Common Operational Datasets Administrative Boundaries (COD ABs) (https://cod.unocha.org/, last access: 15 September 2023) for the Philippines.

4. Feature 24 with the prefix VUL represents the percentage of people in poverty. It was generated from an analysis of the 2012 census.[3]

5. Features 25–36 were all synthesized from Philippines Pre-Disaster Indicators datasets on the Humanitarian Data Exchange (https://data.humdata.org/dataset/philippines-pre-disaster-indicators, last access: 15 September 2023). Feature 25 is simply the number of houses per municipality. We transformed the original values from the municipality to the grid level for this feature using building data as explained in Sect. 3.1. Features 26–34 denote the composition of the housing construction materials. Feature 35 represents the number of vulnerable groups by city/municipality from the DSWD National Household Targeting Office, while feature 36 is based on the number of Pantawid Pamilya (https://pantawid.dswd.gov.ph/, last access: 15 September 2023) beneficiary households. For all these features starting with the prefix VUL, the original source was at the municipality level.

3.3 Additional only grid-level features

In addition to the features described above, we also add features from globally available datasets that were available at

---

[3]Unfortunately, the original dataset and analysis are no longer publicly available.
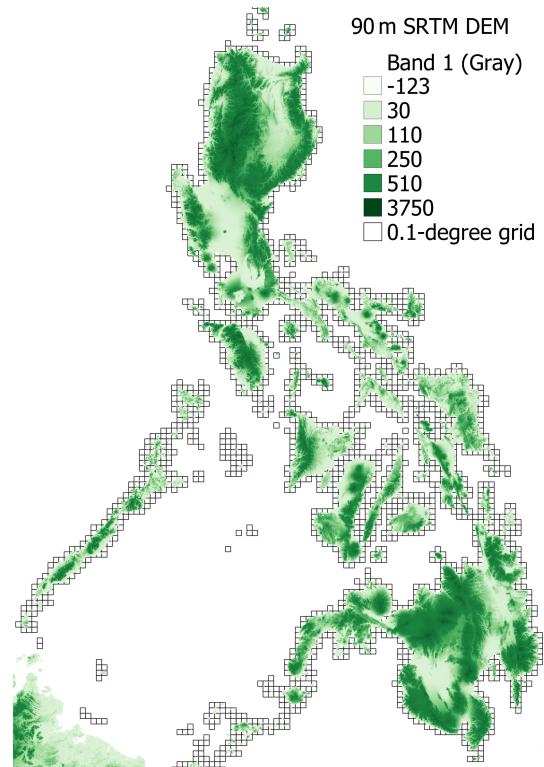

Figure 4. Elevation data from the SRTM database. It shows the elevation at 90 m spatial resolution. Light green indicates lower elevation, while dark green shows high elevation.

the grid level (contributing to the set of features we dub Global+) but sometimes in a different resolution than our 0.1° grid. We describe them below and explain the corresponding transformation if needed.

6. Feature 37 with the prefix VUL corresponds to the Relative Wealth Index (RWI) (https://data.humdata.org/dataset/relative-wealth-index, last access: 15 September 2023), which was mean-aggregated for each grid cell. It originally came as point data, and the corresponding grid value was derived from points contained wholly within a grid cell. Since missing values exist in some grid cells of this feature, we estimated the average of available values over all grid cells. Then, we replaced null values with this average to diminish the impact of missing data and preserve as much as possible the data integrity.

7. Feature 38, the population data (https://ghsl.jrc. ec.europa.eu/download.php?ds=pop, last access: 15 September 2023), is available as a 100 m resolution raster and is aggregated to each grid cell.

8. Features 39–41 represent the proportion of urban, rural, and water areas aggregated similarly to the population data. They are based on the 2025 epoch of the Degree of Urbanisation dataset (https://ghsl.jrc.ec.europa.
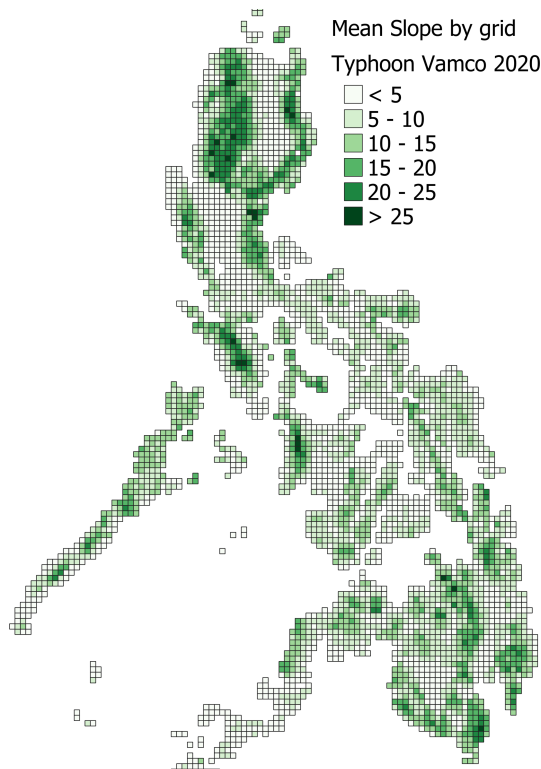
Figure 5. Slope as computed from the SRTM database. The slope is still shown at a 90 m spatial resolution, with the shades of green indicating the steepness of the slope. Light green shows a flatter slope, while dark green shows a steep slope.

Figure 6. Mean slope by grid. The 90 m slope is averaged for each 0.1° grid.

eu/download.php?ds=smod, last access: 15 September 2023) from the Global Human Settlement Layer (GHSL), which classifies settlement typologies and has a 1 km resolution raster. The GHSL dataset provides complete information on human settlements built on satellite imagery and other geospatial data. To calculate the proportion of urban areas for one of our 0.1° grid cells, we take the fraction with 21 or more significant values in the Degree of Urbanisation dataset. Similarly, the proportion of rural areas is the percentage that has values between 11 and 13, and the proportion of water has a percentage value of 10. The sum of these three features add up to 1.

9. Feature 42, finally, is the percentage of damaged houses in the 5 years prior to a typhoon event, calculated as the average of the target variable in the 5 years prior to the disaster event. This value is 0 in the absence of any prior data.

3.4 Feature selection

Selecting the most important features and their relevance in a dataset aids in effectively applying machine learning (ML) algorith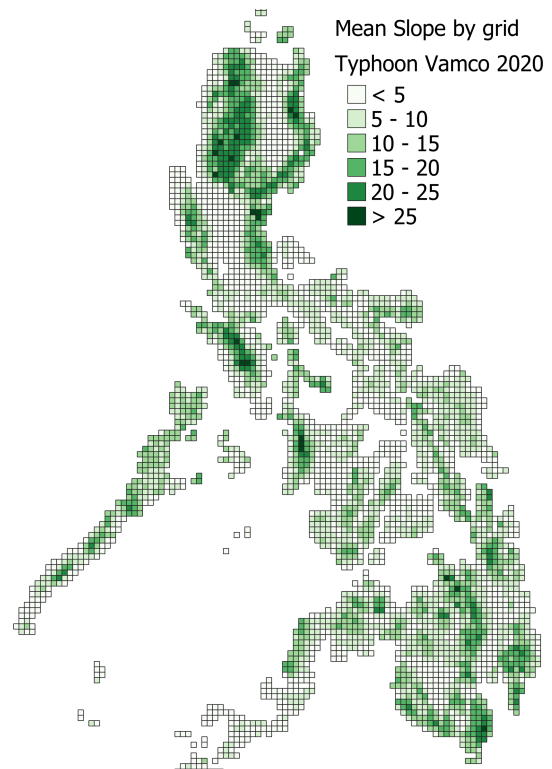ms in real-world scenarios. Therefore, in this study, we use correlation among features to select features that reduce multicollinearity. See Fig. 7 for a visualization of the feature correlations in the municipality dataset. Using this information, we remove features 9 (HAZ_SEC_Bu_p_inSSA), 10 (HAZ_SEC_Bu_p_LS), 14 (HAZ_SEC_Red_per_SSAbldg), 20 (TOP_mean_ruggedness), and 21 (TOP_slope_stdev) in Table 1 from the input municipality dataset since the absolute value of their correlation with other features is larger than 0.99.

3.5 Predictive models

Our models are trained using eXtreme Gradient Boosting (XGBoost), both for regression and classification, a popular tree-based ensemble-learning method, which was also used in the 510 model, which our analysis extends. Additionally, we compared our models' performance with a naive baseline (based on the average of training data) and linear regression and RF. We omit results for the latter two models from the analysis below as they perform slightly more poorly. We describe all the models we used and the corresponding set of features in Table 2.

– M-Local contains municipality-level data with a subset of the original features (Local in Table 1).
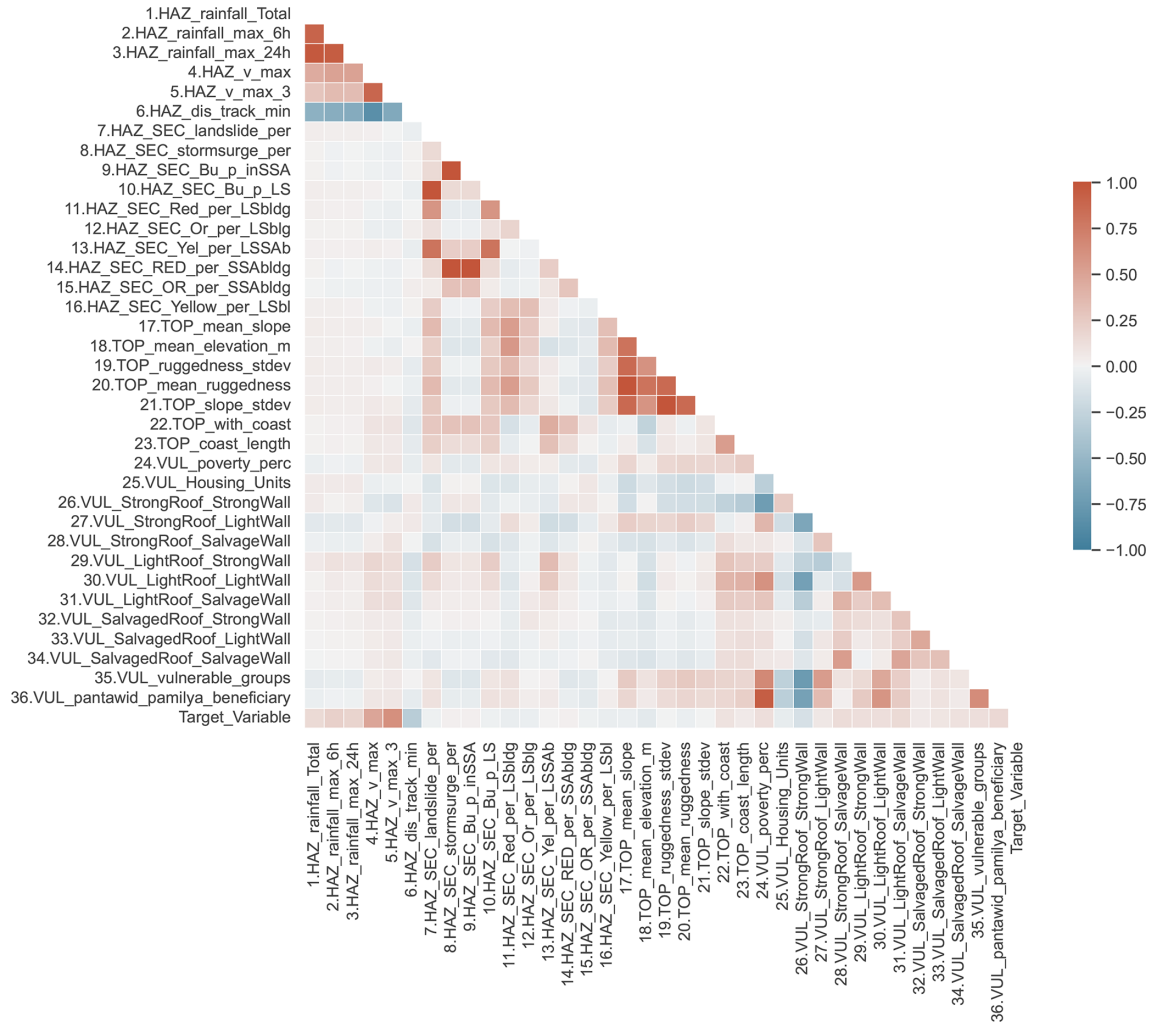
Figure 7. Correlation matrix before removing highly correlated features in the municipality dataset.

Table 2. Table of model description.

Model name	No. of features	Model description	Feature set (see Table 1)
M-Local	31	Municipality-level data with original features	Local
M-Global	12	Municipality-level data with only global features	Global
G-Global	12	Grid-level data with only global features	Global
G-Global+	18	Grid-level data with global and additional features	Global+
2SG-Global+	18	Grid-level data with global and additional features using a two-stage classifier (the model is explained in more detail in Fig. 8)	Global+
M-Naive	0	Municipality-level naive baseline based on the target variable average of the training set	None
G-Naive	0	Grid-level naive baseline only using the target variable average of the training set	None

- M-Global contains municipality-level data with only global features (Global in Table 1).

- G-Global contains grid-level data with only global features (Global in Table 1).

- G-Global+ contains grid-level data with global and additional features (Global+ in Table 1).

- 2SG-Global+ contains grid-level data with global and additional features (Global+ in Table 1) using a two-stage classifier, explained in more detail in Fig. 8.

- M-Naive contains the municipality-level naive baseline that only uses the average of the target variable in the training set at the municipality level.

- G-Naive contains the grid-level naive baseline that only uses the average of the target variable in the training set at the grid level.

We begin our experiments by re-implementing the original 510 model that uses municipality-level features, but, with feature selection, we call this model M-Local. Not all these features are globally available, so we test this model on a global subset of features (M-Global). We then use the features at the grid level and test them in this new resolution (G-Global). In an attempt to improve this model, we take two steps. First, we introduce additional global features called Global+ and test them in G-Global+. Second, we implement a two-stage classifier that handles high-damage data points separately (2SG-Global+). This is another attempt to deal with the high skewness of our target variable.

The flowchart of this final hybrid model (2SG-Global+) is illustrated in Fig. 8. For this model, we first build a binary XGBoost classifier to separate high- and low-damage areas (using a 10 % damage threshold) with undersampling (using 0.1 as the parameter, reducing the majority class to a size 10 times larger than the minority class)[4] to enhance the classification performance by minimizing the false negatives. Then, we train a second XGBoost regression model (XGBoost-highDamage) using only training data from the high-damage areas. The final result of the 2SG-Global+ model is then (based on the outcome of the binary classifier) either given by the G-Global+ model for data classified as potentially low damage or by the XGBoost-highDamage model for the rest of the data classified as potentially high damage.

3.6 Model evaluation

We perform several types of evaluations using the following error metrics: root mean square error (RMSE) and average error (predicted damage − real damage). We report the mean and standard deviation over 20 experiments in each case to average over the variability in the underlying algorithms and sample selections. To have a fair comparison between the models, we evaluate at the municipality level (transforming the results back from the grid level if needed) and only evaluate the data points present in the original municipality dataset used by the 510 model.

We first evaluate all the models mentioned in Sect. 3.5 with a train to test split ratio of 80 : 20 and stratification as explained in Sect. 3.1. Note that because the split does not consider the typhoons, (different) data points from the same

---

[4]We also experimented with other parameter settings as well as oversampling strategies (data not shown). However, the results were slightly worse.

typhoon may be included in both test and train sets. The rationale behind starting with random train–test splits to evaluate our models is that the more realistic case of typhoon-based train–test splits leads to considerable variability in the performance of the models between different runs, as the severity of typhoons is very heterogeneous. This makes it difficult to assess and compare the performance of different models. Furthermore, random train–test splits allow for the stratification of test and training sets by severity bins, achieving more stable results. We can thus better analyze and compare the efficiency of different model types, the feature importance, and the impact of changing from a municipality to a grid-based model.

However, to understand our best-performing models' performance in a real-time use case, we also undertake a walk-forward evaluation and leave-one-out cross-validation (LOOCV), wherein the typhoon timings are preserved. The walk-forward evaluation uses a chronologically ordered set of typhoons, starting with an initial training set of 27 typhoons (approx. 70 % of the data). Each iteration adds a new typhoon to the training set, and the model is tested on the next one (making for 12 iterations for each of the 12 remaining typhoons). The aim is to determine how well the model learns from older typhoons' characteristics to predict the next. We implemented an alternative version, where the oldest typhoon is dropped when adding a new one (making the training window fixed), but as the results were statistically the same, we do not report them here. In the LOOCV, we cycle through all typhoons, using one typhoon as a test set and the others to train the models. This setting makes more data available (allowing the use of "future" data) for training than the walk-forward scenario.

3.7 Model explainability

We employed SHAP (SHapley Additive exPlanations), a game theory approach developed to explain the contribution of each feature to the final output of any ML model (Lundberg and Lee, 2017b). SHAP values provide global and local interpretability, meaning we can assess how much each predictor and observation contributes to the classifier's performance. The local explanations are based on assigning a numerical measure of credit to each input feature. Then, global model insights can be obtained by combining many local explanations from the samples (Lundberg et al., 2019). As mentioned by the authors, the classic Shapley values can be considered "optimal" in the sense that within a large class of approaches, they are the only way to measure feature importance while maintaining several natural properties from cooperative game theory (Lundberg and Lee, 2017a). SHAP's output helps to understand the general behavior of our model by assessing the impact of each input feature in the final decision, thus enhancing the usefulness of our framework.
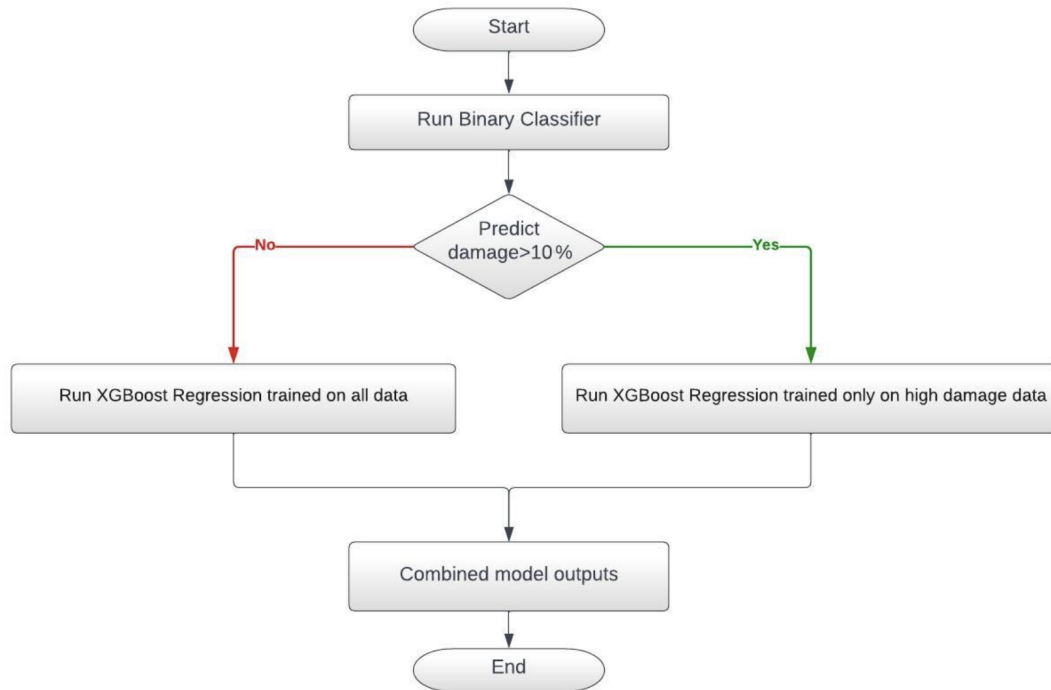
Figure 8. Flowchart of the combined model.

4 Results

This section presents the results from the evaluations described in the previous section. We start with random train–test splits that do not stratify by typhoons. Then, we show the LOOCV and walk-forward settings and finish with an illustrative case study.

4.1 Random test–train split evaluation and regression model performance

Table 3 shows the RMSE (and standard deviation over 20 runs) for the four regression models and the two-stage hybrid model described in Sect. 3.5, as well as the two baseline models which predict the average damage in a municipality/grid as seen in the training data (ignoring all features). We present the results per damage bins and the average over all the test data, which we refer to as the weighted average (recall that the data are heavily skewed towards the first few bins). Also note that when we compute the metric, the predictions of the grid-based models are converted to the municipality level, and only municipalities present in the original data used by the 510 model are considered for a fair comparison across all models.

First, we note that the RMSE score increases proportionally to the bin's interval, meaning those municipalities that experienced more damage also have higher errors associated with the model's prediction. Since the dataset has more data points in the initial bins, we will face a higher standard de-

viation in the latest bins. When we limit the variables from the M-Local model to only those globally available (down to 12 features) in M-Global, the model's performance does not suffer significantly in terms of RMSE. Further, as we add features to our set (G-Global+), the performance improves slightly in the higher damage range when compared to G-Global. Finally, the two-stage model (2SG-Global+) achieves the best RMSE for bin 4, as it is designed to perform slightly worse for the low-damage bins, which results in a weighted average RMSE of 4.73. The table also includes two baselines: one for the municipality and one for the grid level. These achieve a worse performance compared to the proposed models. They perform the best in the middle bin, as the overall average falls into this bin.

Additionally, Table 4 shows the average error achieved by the same models. This is the average difference between estimated and actual damage values, so the model tends to underestimate the real damage when the average error is negative. As we can see, for the five models under analysis, the real damage is overestimated for the first three bins and is underestimated for the last two with the highest damage. This effect is expected due to the skewness of the data. While the average error over all bins (weighted average) remains close to 0 for the municipality-level models, introducing the grid-level increases the models' tendency to underestimate. However, on average, the 2SG-Global+ model corrects the overall bias closer to 0. In particular, we again notice a significant improvement in bin 4.

Table 3. Table of RMSE per bin and the weighted average for the five proposed models and two baselines (standard deviation over 20 runs in parentheses).

Bin interval	M-Local	M-Global	G-Global	G-Global+	2SG-Global+	M-Naive	G-Naive
1. [0, 0.00009]	0.27 (0.05)	0.35 (0.11)	0.27 (0.10)	0.24 (0.08)	0.39 (±0.20)	2.22 (0.01)	0.83 (0.00)
2. (0.00009, 1]	2.10 (0.34)	2.30 (0.27)	1.60 (0.16)	1.50 (0.13)	1.94 (0.17)	2.03 (0.02)	0.68 (0.01)
3. (1, 10]	4.37 (0.46)	4.45 (0.54)	4.57 (0.48)	4.63 (0.54)	5.64 (0.59)	2.82 (0.16)	3.69 (0.12)
4. (10, 50]	13.47 (1.10)	14.58 (1.01)	14.27 (1.05)	14.02 (0.66)	12.48 (0.90)	24.81 (1.15)	25.34 (0.92)
5. (50,100]	27.93 (4.98)	30.54 (5.69)	33.51 (3.89)	31.62 (3.50)	31.67 (3.97)	60.88 (3.39)	63.97 (2.35)
Weighted average	4.42 (0.29)	4.77 (0.32)	4.82 (0.28)	4.71 (0.20)	4.73 (0.28)	8.03 (0.24)	8.25 (0.24)
Total features	31	12	12	18	18	0	0

Table 4. Table of average error per bin and the weighted average for the five proposed models and two baselines (standard deviation over 20 runs in parentheses).

Bin interval	M-Local	M-Global	G-Global	G-Global+	2SG-Global+	M-Naive	G-Naive
1. [0, 0.00009]	0.08 (0.01)	0.08 (0.02)	0.03 (0.01)	0.03 (0.01)	0.04 (0.01)	2.22 (0.01)	0.83 (0.00)
2. (0.00009, 1]	0.89 (0.07)	1.12 (0.09)	0.63 (0.06)	0.58 (0.03)	0.67 (0.05)	2.01 (0.02)	0.64 (0.01)
3. (1, 10]	0.89 (0.28)	0.94 (0.34)	0.00 (0.28)	0.10 (0.25)	1.00 (0.35)	−1.42 (0.16)	−2.80 (0.12)
4. (10, 50]	−6.28 (1.32)	−7.16 (1.36)	−7.13 (1.00)	−6.66 (0.92)	−4.53 (0.97)	−21.77 (1.18)	−22.57 (0.81)
5. (50,100]	−20.55 (6.12)	−24.57 (6.40)	−25.20 (3.93)	−23.49 (3.52)	−25.39 (3.97)	−59.97 (3.03)	−62.72 (2.16)
Weighted average	0.01 (0.10)	0.02 (0.11)	−0.33 (0.06)	−0.30 (0.06)	−0.06 (0.09)	−0.03 (0.07)	−1.43 (0.05)
Total features	31	12	12	18	18	0	0

Next, we explore the feature importance of the globally available variables (column Global+ in Table 1). Figure 9 shows the bee swarm plot of the SHAP values for the G-Global+ model. It allows us to observe the impact of each feature on the model output. For instance, among the most critical variables, high values (red points) of the wind speed feature indicate a high positive contribution to the prediction (positive SHAP value). High values of the 6 h maximum rainfall (in red) are positively associated with damage, while lower ones (in purple) have a negative one. This effect gets diluted when the rainfall aggregation is for 24 h, where we can also observe an increased negative impact of high feature values. Interestingly, the track distance can have a positive and a negative impact, especially when its values are low. Furthermore, historical data (Percent_houses_damaged_5years) mostly positively impact the prediction. The elevation feature (TOP_mean_elevation_m) does not provide a clear picture alone, while the mean slope feature shows that flat areas are more likely to receive damage than others. We also observe a positive impact of the coast length feature on damage estimation since coastal areas are more prone to storm surges and landslides.

Further, social–demographic features provide a window into the unequal distribution of damage caused to the population. Variables concerning total houses and urban and rural measures indicate that the areas with fewer houses (less urbanization) are affected more than those in the cities. The RWI also shows that those affected tend to come from eco-

nomically disadvantaged areas. In summary, the most critical features involve the characteristics of the typhoon in terms of wind and precipitation. Although contributing less to the model performance, the conditions on the ground, such as population, urbanization type, or the RWI, provide a clear directional signal on how they influence the expected damage.

4.2 Evaluation by typhoon

In this section, we now evaluate our best model (2SG-Global+) in a more realistic setting with train–test splits with stratification by typhoon in two ways: iterative walk-forward evaluation and leave-one-out cross-validation (LOOCV). Figure 10 gives a graphical representation of these two typhoon-based stratification strategies explained in detail in Sect. 3.6. For the sake of comparison, we show the LOOCV evaluation here only for the same 12 typhoons used for the walk-forward evaluation – this makes these results different from those in the previous section. The overall performance is slightly better in LOOCV compared to the walk-forward setting, which makes sense, as it has access to more training data.

Table 5 shows the RMSE, and Table 6 shows the average error for the 2SG-Global+ model, the M-Local model, and G-Naive model (i.e., the average historical damage), evaluated using the two methods. Compared to G-Naive, our hybrid 2SG-Global+ model achieves a substantially better
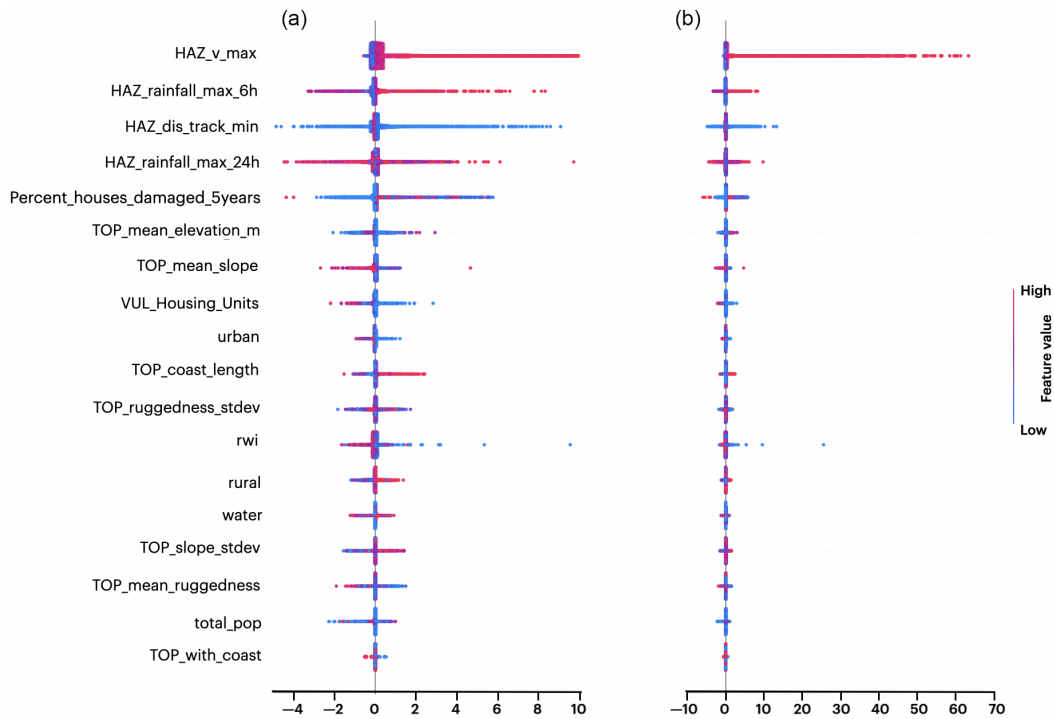
Figure 9. SHAP values for variables in the G-Global+ model, sorted by the importance of all the globally available features. Panel **(b)** shows the whole scale of SHAP values, while panel **(a)** shows a reduced x-axis range for better data visualization.
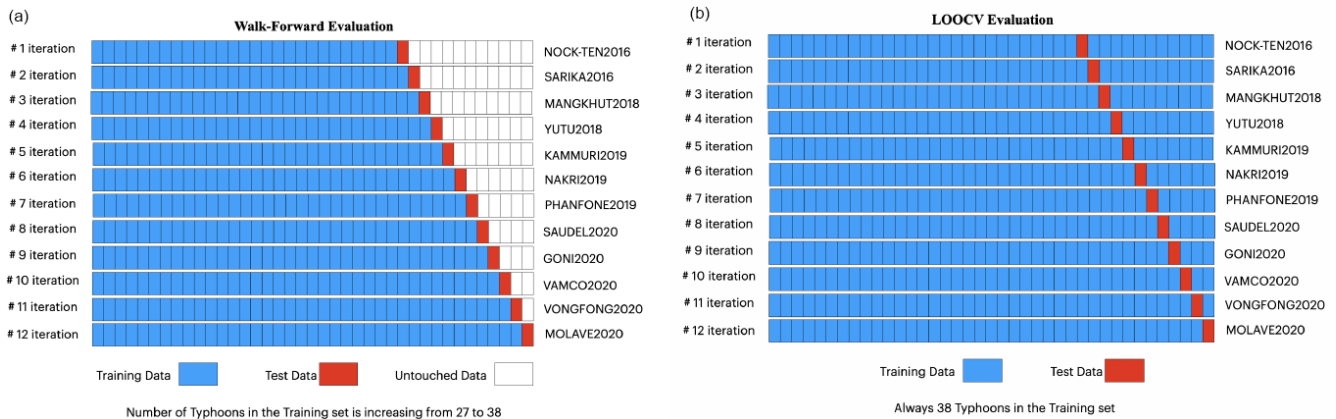

Figure 10. Schematic diagram of the **(a)** walk-forward and **(b)** LOOCV typhoon-based evaluation to illustrate how the dataset is split into the training and test sets.

RMSE in the higher damage bins, especially at the highest range of (50, 100], having an RMSE of 33.61 (±22.30) compared to 57.02 (±6.19) for G-Naive (LOOCV evaluation). Additionally, the weighted average RMSE for the walk-forward and LOOCV scenarios of the 2SG-Global+ model are 2.55 (±1.98) and 2.48 (±1.93), which indicate a better performance than the M-Local model with an RSME of 2.74 (±1.66) and 2.64 (±1.66), respectively. For the first three bins, the 2SG-Global+ model has the lower RMSE,

while for the last two bins (high-damage data), M-Local performs slightly better than the 2SG-Global+ model. Furthermore, besides the highest-damage bin, the proposed model improves the average error.

Figures 11 and 12 show the performance of the two models only in grid cells with damage of > 10, evaluated using LOOCV (calculated for all typhoons having such high-damage impact instead of just the 12 used in Tables 5 and 6). We find that, for most typhoons, the error is substantially

Table 5. RMSE per bin and the weighted average for the M-Local, 2SG-Global+, and G-Naive models (with the same dataset size) in walk-forward and leave-one-out cross-validation (LOOCV) evaluation.

Bin interval	M-Local		2SG-Global+		G-Naive	
	Walk-forward	LOOCV	Walk-forward	LOOCV	Walk-forward	LOOCV
1. [0, 0.00009]	0.22 (0.16)	0.25 (0.17)	0.10 (0.07)	0.11 (0.08)	0.91 (0.03)	0.84 (0.01)
2. (0.00009, 1]	1.89 (1.50)	1.82 (1.41)	1.32 (1.84)	1.37 (2.08)	0.76 (0.08)	0.69 (0.08)
3. (1, 10]	5.61 (3.12)	5.16 (2.32)	4.82 (3.42)	4.86 (3.45)	3.41 (1.10)	3.47 (1.12)
4. (10, 50]	11.24 (2.67)	10.41 (4.58)	12.89 (3.08)	12.32 (3.08)	16.33 (3.94)	16.40 (3.93)
5. (50, 100]	29.39 (16.72)	33.24 (11.17)	31.05 (21.92)	33.61 (22.30)	56.95 (6.24)	57.02 (6.19)
Weighted average	2.74 (1.66)	2.64 (1.66)	2.55 (1.98)	2.48 (1.93)	2.85 (2.00)	2.84 (2.04)
Total features	31		18		0	
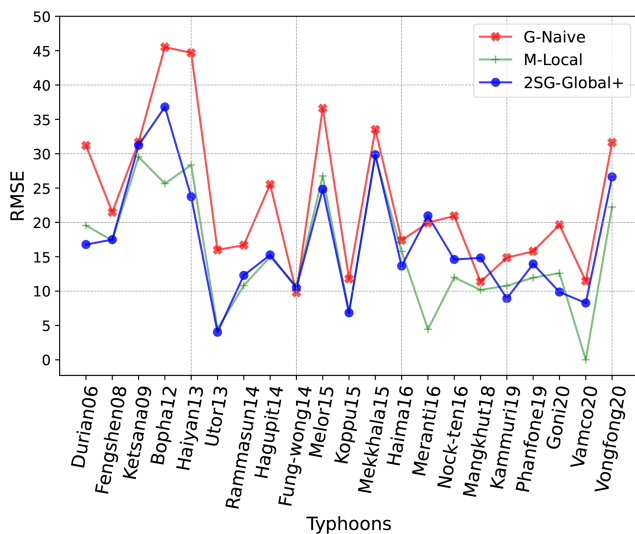
Figure 11. RMSE for areas with damage of $> 10\,\%$ by typhoon (LOOCV, only typhoons with high-damage areas shown).
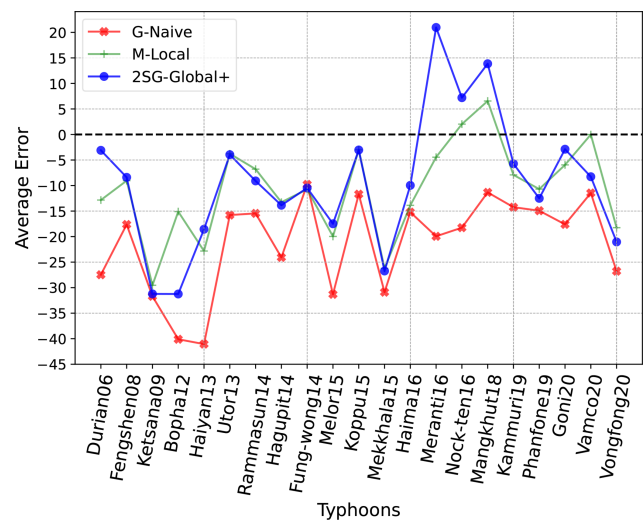
Figure 12. Average error for areas with damage of $> 10\,\%$ by typhoon (LOOCV, only typhoons with high-damage areas shown).

reduced. The average error tells us that the 2SG-Global+ model's predictions are less pessimistic; that is, the model underestimates the damage to a lesser extent than what we would have predicted based on the historical baseline (G-Naive) and, in some cases, even overestimates it. In general, the G-Naive baseline model has the worst RMSE. It also has the worst average error for all typhoons compared to the two other models. For some typhoons like Meranti16 and Vamco20, the M-Local model has the lowest RMSE, while for the earlier typhoons, such as Haiyan13, Utor13, Rammasun14, and a few more, the performance of 2SG-Global+ is very similar to M-Local. It was even better in some cases, like Bopha12 (the most severe), which is remarkable given that M-Local includes 31 features and 2SG-Global+ only has 18 features.

4.3 Action trigger application

The above comparison, however, needs to reflect the usefulness of these models in decision-making during emergencies. The real-world application case would be to predict municipalities where the damage will be more significant than $10\,\%$, so an appropriate action can be triggered. Using the output of our models for this classification task, we show in Table 7 the corresponding number of true-positive (TP), false-positive (FP), and false-negative (FN), as well as precision (P), recall (R), and F1, scores for the G-Naive baseline and the average of 20 runs of the 2SG-Global+ and the M-Local models. The G-Naive model never predicts the damage will be over $10\,\%$, as most of the data skew to minor damage. This results in a low RMSE because, indeed, for most data points, this prediction is correct but would never trigger appropriate action. Alternatively, M-Local identifies the municipalities having damage of over $10\,\%$ with a precision of 0.60 and a recall of 0.57. The 2SG-Global+ model then improves this

Table 6. Average error per bin and the weighted average for the M-Local, 2SG-Global+, and G-Naive models (with the same dataset size) in walk-forward and leave-one-out cross-validation (LOOCV) evaluation.

	M-Local		2SG-Global+		G-Naive	
Bin interval	Walk-forward	LOOCV	Walk-forward	LOOCV	Walk-forward	LOOCV
1. [0, 0.00009]	0.07 (±0.08)	0.10 (0.09)	0.02 (0.05)	0.02 (0.05)	0.91 (0.03)	0.84 (0.01)
2. (0.00009, 1]	1.00 (1.02)	1.10 (1.17)	0.51 (1.03)	0.67 (1.40)	0.71 (0.11)	0.63 (0.11)
3. (1, 10]	2.07 (2.71)	1.84 (2.26)	0.69 (3.17)	0.95 (3.34)	−2.68 (0.97)	−2.76 (0.99)
4. (10, 50]	−4.82 (6.83)	−4.16 (6.95)	−2.89 (9.83)	−3.06 (9.40)	−15.27 (3.18)	−15.36 (3.17)
5. (50, 100]	−29.39 (16.72)	−33.24 (11.17)	−31.05 (21.92)	−33.61 (22.30)	−56.95 (6.24)	−57.02 (6.19)
Weighted average	0.35 (0.58)	0.35 (0.57)	0.03 (0.87)	0.07 (0.84)	−0.15 (0.98)	−0.22(0.99)
Total features	31		18		0	

performance by increasing the number of true positives and decreasing the number of false positives and false negatives. This results in a value of 6.9 %. Overall, the F1 measure of the proposed model is the best at 0.65 (an 11.5 % improvement).

In a thought experiment, if decision-makers would use the output of 2SG-Global+, instead of that of M-Local, 41 more municipalities (an increase of 16.1 %) experiencing greater than 10 % damaged houses would receive relief (more true positives, fewer false negatives), and at the same time four fewer municipalities (a decrease of 2.3 %) with damage not exceeding the threshold would not receive aid, saving resources (fewer false positives).

In summary, in this real-world scenario, our model improves resource allocation by better targeting the affected areas where early actions or AAs will be deployed, increasing the correctly predicted damaged areas and reducing false alarms.

4.4 Case study

To illustrate the behavior of the 2SG-Global+ model and compare it with the M-Local model, we visualize the prediction results at the municipality level for a single typhoon estimated by these two models. We chose Typhoon Melor (Melor15), which struck the Philippines in December 2015, since it was classified as a very strong typhoon by the Japan Meteorological Agency and a category-4-equivalent typhoon by the Joint Typhoon Warning Center (JTWC). A typhoon equivalent to a category-4 typhoon on the Saffir–Simpson hurricane wind scale (SSHWS) (Taylor et al., 2010) is considered a "super typhoon", with a warning that "well-built framed homes can sustain severe damage with loss of most of the roof structure and/or some exterior walls. Most trees will be snapped or uprooted, and power poles will be downed. Fallen trees and power poles will isolate residential areas. Power outages will last weeks to possibly months. Most of the area will be uninhabitable for weeks or months."
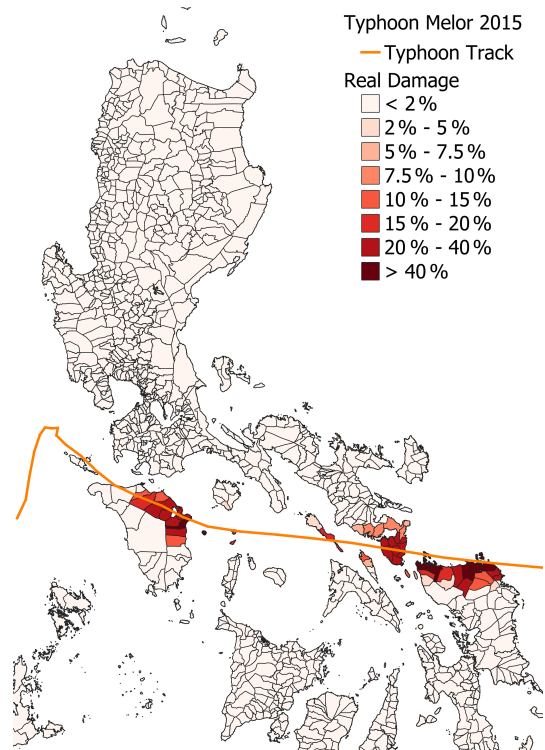

Figure 13. The real damage per municipality reported for Typhoon Melor in 2015.

Figure 13 shows the typhoon track (orange line) and actual damage at the municipality level during this typhoon. To have a fair comparison between the 2SG-Global+ and the M-Local models, we transformed the results of the 2SG-Global+ from the grid to the municipality level. We used only the data from the municipalities present in the original municipality dataset used by the 510 model.

Figures 14 (for 2SG-Global+) and 15 (for M-Local) show the predicted damage, and Figs. 16 and 17 show the corresponding errors in the two models for Typhoon Melor. For individual municipalities, the models either underesti-

Table 7. Performance in predicting municipalities with damage of $> 10\%$ tested using LOOCV. True-positive (TP), false-positive (FP), false-negative (FN), precision, recall, and F1 scores for the 2SG-Global+ (average of 20 runs) and M-Local models and the G-Naive baseline.

	TP	FP	FN	Precision	Recall	F1
G-Naive baseline	0	0	447	0	0	0
M-Local	254	173	193	0.595	0.568	0.581
2SG-Global+	295	169	152	0.636	0.660	0.648
Improvement	16.14%	−2.31%	−21.24%	6.89%	16.17%	11.48%
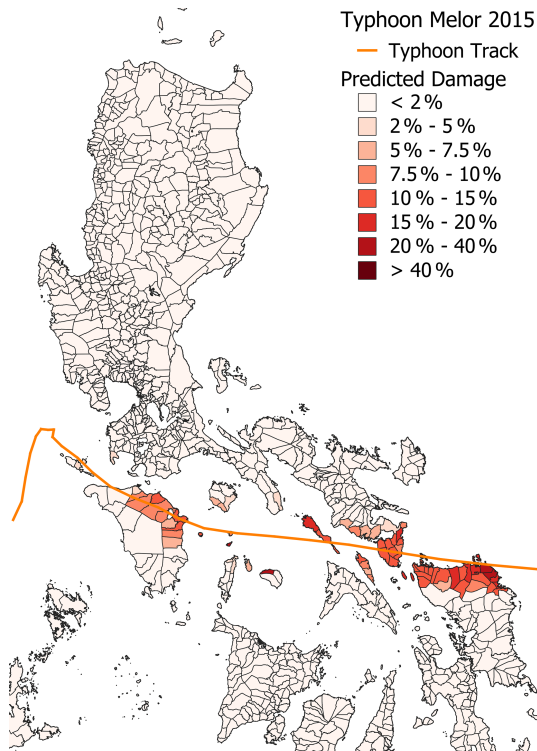
Figure 14. The damage as predicted by the 2SG-Global+ model for Typhoon Melor aggregated from the 0.1° grid to the municipality level.
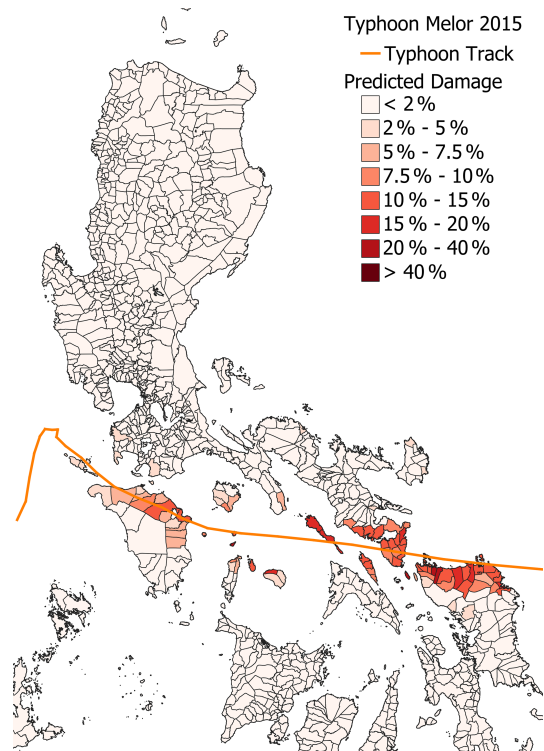
Figure 15. The damage predicted by the M-Local model for Typhoon Melor.

mate the damage (blue squares) or, in a few cases, overestimate it (red), but, in general, the areas with predicted damage coincide or are close to the affected zones. The average error in 2SG-Global+ for Melor is approximately −0.5, slightly underestimating the impact of the typhoon on average, while, for the M-Local model, this error is considerably larger (−2.98).

Still, we generally observe very similar values, with few noticeable differences between the two models in these figures. However, going back to Figs. 11 and 12 we do observe that the 2SG-Global+ model performs slightly better with a reduction in RMSE of 1.9 (−7.2%) and average error of 2.5 (−12.5%) in the high-damage areas (municipalities with damage of $> 10\%$). This was also observed in the action trigger application analyzed in the previous subsection,

where we found that for Typhoon Melor, the 2SG-Global+ model correctly identified 35 municipalities as highly damaged (only missing 8). In contrast, the M-Local model only identified 25 of them.

5 Discussion and conclusions

In this study, we created 2SG-Global+, a grid-based typhoon damage prediction model for the Philippines. It uses fewer features than the original municipality-based 510 model (Teklesadik et al., 2023) while conserving performance in terms of RMSE. The features of our grid-based model have all been selected from an open-access global database, which facilitates the possibility of extending the grid-based model to different geographical contexts. When applied as a clas-
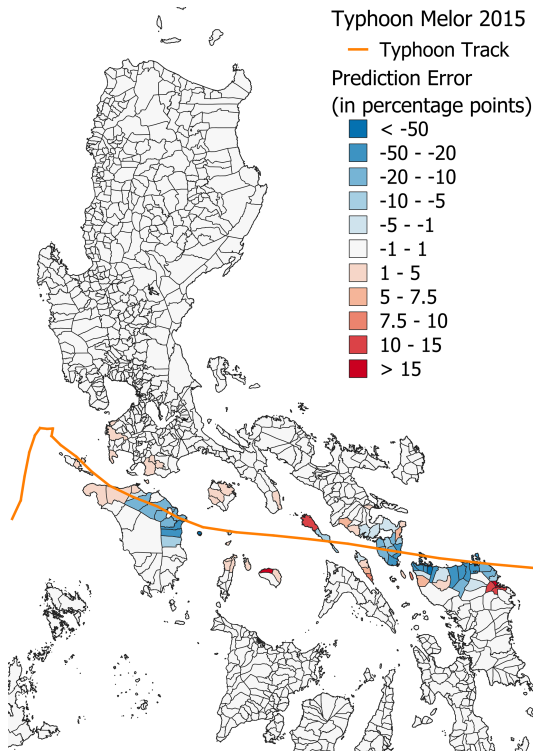
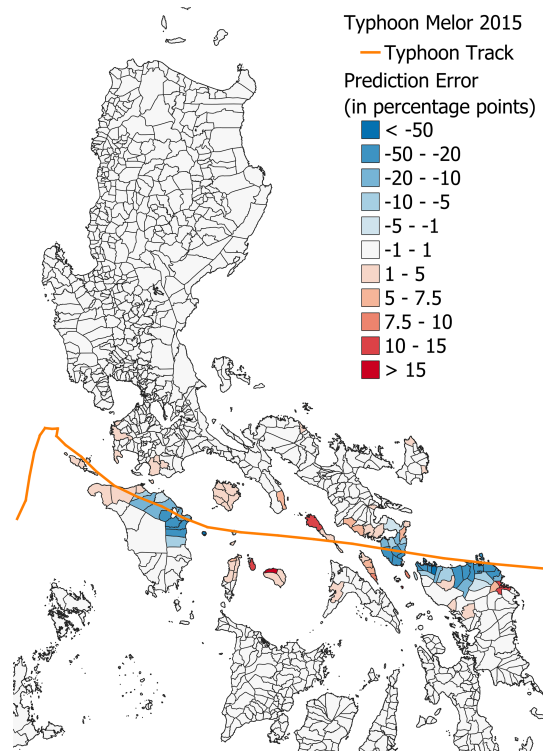**Figure 16.** The error in the 2SG-Global+ model aggregated by municipality (predicted − real).

Figure 17. The error in the M-Local model per municipality (predicted − real).

sification model for high-damage areas (more than 10 % of housings destroyed) and despite excluding hazard and vulnerability features only available in the Philippines, our hybrid 2SG-Global+ model achieves an F1 of 0.648, which surpasses a variant of the 510 model (M-Local) with F1 of 0.581. Our model shows a higher true-positive rate (295 instead of 254 from M-Local) and a lower false-negative rate (152 instead of 193). The 2SG-Global+ model even slightly outperforms M-Local, respecting the false-positive rate (169 instead of 173), meaning fewer resources would be wasted. Furthermore, the availability of the model results in a 0.1° grid, allowing for a more targeted AA approach.

In the Philippines, at the moment this paper is written, there is a partly human-out-of-the-loop (510 model to select municipalities) and a partly human-in-the-loop approach (barangay validation committee that selects the program participants) (van den Homberg et al., 2020) in place for AA. With a grid-level model, the barangays (smaller than municipalities) can be better targeted by aggregating the grid cells into barangays instead of the municipality level. It should be noted that the grid-cell model can distribute some of its predictions to municipalities outside the municipalities of the target training data, with two consequences. It allows for the uncovering of areas that might have been overlooked in the data collection (e.g., areas with mild damage that have not been reported but are helpful to train the model). However, it also might allocate damage to areas of minor importance

(e.g., neighboring villages with very few houses). Furthermore, this data redistribution to the grid level leads to a more fine-grained and uniform spatial data distribution. This augmentation of data points (as shown in Fig. 2) quite possibly has a positive influence. Additionally, the inclusion of terrain-type features has undoubtedly also helped in improving model performance.

Our study demonstrates that creating a grid-level impact-based forecasting model using global features for the Philippines is possible. Further research will focus on applying the grid-level approach to other TC-prone countries so that the replicability of the model can be tested. Whereas data on the features of the grid-based model are available for other countries from global repositories, this will not be the case for the target data. The aggregation level of the target data available for other countries will differ. These data might be more detailed in some data-richer countries, making the model less sensitive to disaggregation by using building footprint data. Also, our geospatial workflow could be audited for biases (Masinde et al., 2023). Efforts are underway to identify biases within satellite building datasets like Open Street Map, Google, and Microsoft Building Footprints to specific attributes such as vulnerability (Gevaert, 2022). It will be essential to assess the sensitivity of the grid-level model to these biases. In our research, the target data have been damage to houses, but damage to other assets can be used. For example, Boeke et al. (2019) and van Brussel (2021) developed

a model for predicting damage to rice fields in the Philippines initially at the province level and later at the municipality level. Damage to rice fields will require a different way of disaggregating. Land-use/land-cover data could be used to assign rice damage to a specific grid cell.

The models in our research are trained with observed TC data. It is important to emphasize that the performance of an operational impact-based forecasting model is determined not only by the performance of the model itself but also by the forecast skill of the real-time hazard forecast that goes into the model. For example, the position error for 3 d of European Centre for Medium-Range Weather Forecasts (ECMWF) ensemble forecasts averaged 150–200 km over the last few years (MacLeod et al., 2021). Also, the Philippine Red Cross requires 72 h to implement early actions such as distributing house-strengthening kits. However, in the Philippines, of the 522 TCs that made landfall from 1951--2020, 146 TCs (28 %) underwent rapid intensification, defined as an increase of the upper 95th percentile in TC maximum winds in a 24 h period. Of this 28 %, 82 % had at least typhoon intensity (Tierra and Bagtasa, 2023; Fudeyasu et al., 2018). This means that the threshold level of any impact-based forecasting model will not be reached at 72 h. The operational 510 model uses the forecasts from ECMWF as they represent the state of the art in TC forecasting (MacLeod et al., 2021) and can feed directly into an automated workflow. However, the forecasts from the Philippine Atmospheric, Geophysical and Astronomical Services Administration (PAGASA, 2023) are contextualized with their local knowledge, and updates are often available faster. Therefore, further research will explore the adoption of the PAGASA forecasts. When replicating the grid-level model to other countries, a forecast skill assessment of the different forecasts available for that country has to be done.

Apart from the primary hazard, a possible future improvement in our model may come in the form of dynamic modeling of the consecutive or secondary hazards caused by a TC. For example, for storm surge, dynamic models, such as the Global Tide and Surge Model, are being developed (Bloemendaal et al., 2019). Hsu et al. (2023) analyzed the total water levels (TWLs), defined as the combination of astronomic tides, mean sea level, storm surge, and wave runup for three TCs and were able to reproduce this using, among others, the Coupled Ocean–Atmosphere–Wave–Sediment Transport (COAWST) modeling system (Warner et al., 2010). Incorporating these dynamic models into an ML model might improve the secondary hazard features used in grid- and municipality-based models. The new technologies being developed as part of Digital Earth (Annoni et al., 2023) can play a role here.

With our novel model, we are able to increase the number of true positives so that decision-makers can distribute the limited resources better to those who will suffer from more damage. Apart from considering the purely technical performance of our grid-level model, there are opportunities and challenges in adopting an artificial-intelligence-based model by decision-makers (Kbah and Gralla, 2023). A clear opportunity is that the grid-level model uses features that can be the same across countries, which will benefit consistency and comparability. Also, a grid-level model based on global features can be more easily rolled out to new countries, requiring less time and fewer resources. A challenge might be that models based on artificial intelligence (AI) are more of a black box to users with limited data and digital training than expert or rule-based trigger models. For example, setting a threshold might be less intuitive for an XGBoost model than a model primarily based on wind speed. The Red Cross and Red Crescent National Societies in Bangladesh and Mozambique currently use, for example, a relatively straightforward trigger model based on combining a wind speed forecast with vulnerability information (Sedhain et al., 2023). Bierens et al. (2020) explain the importance of an impact-based forecasting model's legitimacy, accountability, and ownership. The knowledge exchange between the developer and the end users of the models falls short if it is just seen as a matter of technology transfer. Instead, co-creation is essential to incorporate the end user's needs fully.

To conclude, relying on globally available data sources and working at the grid level holds the potential to render an ML-based impact model generalizable and transferable to locations outside of the Philippines. The grid-level model can contribute to developing an impact-based forecasting model in a country that still needs to develop a local one. The long-term adoption of our model based on AI may take place by forming an additional source of information next to more expert-based or local models of a government's AA pipeline. Future research will focus on the validation of the model in other countries. Also, UN OCHA and the International Red Cross and Red Crescent Movement aim to gain experience by running the grid-level model parallel to existing trigger models. Expanding the application of this transferable TC model to other countries will facilitate the scaling up of anticipatory action for TCs.

Author contributions. Conceptualization: MvdH, LM, KK, DP, MLT; data curation: AT, PN; investigation: MK, AK, YM; writing – original draft preparation: MK, AK, YM; writing – review and editing: MK, MvdH, KK, AK, YM, PN, DP, MLT. All authors reviewed the results and approved the final version of the manuscript.

References

Annoni, A., Eremchenko, E., Giuliani, G., Strobl, J., and Chen, M.: Digital earth: yesterday, today, and tomorrow, Int. J. Digit. Earth, 16, 1022–1072, 2023.

Anticipation Hub: Anticipatory Action in 2022: A Global Overview, https://www.anticipation-hub.org/download/file-3249 (last access: 25 April 2023), 2022.

Atwii, F., Sandvik, K. B., Kirch, L., Paragi, B., Radtke, K., Schneider, S., and Weller, D.: World Risk Report, https://weltrisikobericht.de/wp-content/uploads/2022/09/WorldRiskReport-2022_Online.pdf (last access: 13 October 2023), 2022.

Baldwin, J. W., Lee, C.-Y., Walsh, B. J., Camargo, S. J., and Sobel, A. H.: Vulnerability in a Tropical Cyclone Risk Model: Philippines Case Study, Weather Clim. Soc., 15, 503–523, https://doi.org/10.1175/WCAS-D-22-0049.1, 2023.

Bierens, S., Boersma, K., and van den Homberg, M. J.: The legitimacy, accountability, and ownership of an impact-based forecasting model in disaster governance, Politics and Governance, 8, 445–455, 2020.

Bloemendaal, N., Muis, S., Haarsma, R. J., Verlaan, M., Irazoqui Apecechea, M., de Moel, H., Ward, P. J., and Aerts, J. C.: Global modeling of tropical cyclone storm surges using high-resolution forecasts, Clim. Dynam., 52, 5031–5044, 2019.

Bloemendaal, N., De Moel, H., Muis, S., Haigh, I. D., and Aerts, J. C.: Estimation of global tropical cyclone wind speed probabilities using the STORM dataset, Sci. Data, 7, 377, https://doi.org/10.1038/s41597-020-00720-x, 2020.

Bloemendaal, N., de Moel, H., Martinez, A. B., Muis, S., Haigh, I. D., van der Wiel, K., Haarsma, R. J., Ward, P. J., Roberts, M. J., Dullaart, J. C. M., and Aerts, J. C. J. H.: A globally consistent local-scale assessment of future tropical cyclone risk, Science Advances, 8, eabm8438, https://doi.org/10.1126/sciadv.abm8438, 2022.

Boeke, S., van den Homberg, M., Teklesadik, A., Fabila, J., Riquet, D., and Alimardani, M.: Towards predicting rice loss due to typhoons in the Philippines, Int. Arch. Photogramm., 42, 63–70, 2019.

Boettle, M., Kropp, J. P., Reiber, L., Roithmeier, O., Rybski, D., and Walther, C.: About the influence of elevation model quality and small-scale damage functions on flood damage estimation, Nat. Hazards Earth Syst. Sci., 11, 3327–3334, https://doi.org/10.5194/nhess-11-3327-2011, 2011.

Chaves-Gonzalez, J., Milano, L., Omtzigt, D.-J., Pfister, D., Poirier, J., Pople, A., Wittig, J., and Zommers, Z.: Anticipatory action: Lessons for the future, Frontiers in Climate, 4, 932336, https://doi.org/10.3389/fclim.2022.932336, 2022.

Chen, R., Wang, X., Zhang, W., Zhang, W., Zhu, X., Li, A., and Yang, C.: A hybrid CNN-LSTM model for typhoon formation forecasting, Geoinformatica, 23, 375–396, https://doi.org/10.1007/s10707-019-00355-0, 2019.

Cinco, T. A., de Guzman, R. G., Ortiz, A. M. D., Delfino, R. J. P., Lasco, R. D., Hilario, F. D., Juanillo, E. L., Barba, R., and Ares, E. D.: Observed trends and impacts of tropical cyclones in the Philippines, Int. J. Climatol., 36, 4638–4650, 2016.

DSWD Central Office: Amendment to memorandum circular no.19 series of 2018 on the guidelines in the implementation of the emergency shelter assistance (ESA) for the typhoon "Ompong" – Affected households with damaged houses, https://www.dswd.gov.ph/issuances/MCs/MC_2018-019.pdf (last access: 13 October 2023), 2019.

Eilander, D., Couasnon, A., Leijnse, T., Ikeuchi, H., Yamazaki, D., Muis, S., Dullaart, J., Winsemius, H. C., and Ward, P. J.: A globally-applicable framework for compound flood hazard modeling, EGUsphere [preprint], https://doi.org/10.5194/egusphere-2022-149, 2022.

EM-DAT: The International Disaster Database, Centre for Research on the Epidemiology of Disasters, https://www.emdat.be/ last access: 13 October 2023), 2022.

Fudeyasu, H., Ito, K., and Miyamoto, Y.: Characteristics of tropical cyclone rapid intensification over the western North Pacific, J. Climate, 31, 8917–8930, 2018.

Geiger, T., Frieler, K., and Bresch, D. N.: A global historical data set of tropical cyclone exposure (TCE-DAT), Earth Syst. Sci. Data, 10, 185–194, https://doi.org/10.5194/essd-10-185-2018, 2018.

Gettelman, A., Bresch, D. N., Chen, C. C., Truesdale, J. E., and Bacmeister, J. T.: Projections of future tropical cyclone damage with a high-resolution global climate model, Climatic Change, 146, 575–585, 2018.

Gevaert, C. M.: Finding biases in geospatial datasets in the Global South–are we missing vulnerable populations?, in: 41st EARSeL Symposium 2022: Earth Observation for Environmental Monitoring, 13–16 September 2022, Paphos, Cyprus, https://research.utwente.nl/en/publications/finding-biases-in-geospatial-datasets-in-the-global-south-are-we- (last access: 13 October 2023), 2022.

Hallegatte, S., Vogt-Schilb, A., Bangalore, M., and Rozenberg, J.: Unbreakable: building the resilience of the poor in the face of natural disasters, World Bank Publications, ISBN 978-1-4648-1003-9, https://doi.org/10.1596/978-1-4648-1003-9, 2016.

Harrison, S. E., Potter, S. H., Prasanna, R., Doyle, E. E., and Johnston, D.: Identifying the impact-related data uses and gaps for hydrometeorological impact forecasts and warnings, Weather Clim. Soc., 14, 155–176, 2022.

Holland, G.: A revised hurricane pressure–wind model, Mon. Weather Rev., 136, 3432–3445, 2008.

Holland, G. J.: An analytic model of the wind and pressure profiles in hurricanes, Mon. Weather Rev., 108, 1212–1218, 1980.

Hou, H., Yu, S., Wang, H., Xu, Y., Xiao, X., Huang, Y., and Wu, X.: A hybrid prediction model for damage warning of power transmission line under typhoon disaster, IEEE Access, 8, 85038–85050, 2020.

Hsu, C.-E., Serafin, K., Yu, X., Hegermiller, C., Warner, J. C., and Olabarrieta, M.: Total water levels along the South Atlantic Bight during three along-shelf propagating tropical cyclones: relative contributions of storm surge and wave runup, Nat. Hazards Earth Syst. Sci. Discuss. [preprint], https://doi.org/10.5194/nhess-2023-49, in review, 2023.

Jones, J. N., Bennett, G. L., Abancó, C., Matera, M. A. M., and Tan, F. J.: Multi-event assessment of typhoon-triggered landslide susceptibility in the Philippines, Nat. Hazards Earth Syst. Sci., 23, 1095–1115, https://doi.org/10.5194/nhess-23-1095-2023, 2023.

Kbah, Z. and Gralla, E.: Understanding Enablers and Barriers for Deploying AI/ML in Humanitarian Organizations: the Case of DRC's Foresight, in: Proceedings of the IISE Annual Conference & Expo 2023, 21–23 May 2023, New Orleans, Louisiana, USA, ISBN 9781713877851, 2023.

Kim, J.-M., Son, K., and Kim, Y.-J.: Assessing regional typhoon risk of disaster management by clustering typhoon paths, Environ. Dev. Sustain., 21, 2083–2096, 2019.

Kim, J.-S., Chen, A., Lee, J., Moon, I.-J., and Moon, Y.-I.: Statistical prediction of typhoon-induced rainfall over China using historical rainfall, tracks, and intensity of typhoon in the Western North Pacific, Remote Sensing, 12, 4133, https://doi.org/10.3390/rs12244133, 2020.

Kooshki Forooshani, M., van den Homberg, M., Kalimeri, K., Kaltenbrunner, A., Mejova, Y., Milano, L., Ndirangu, P., Paolotti, D., Teklesadik, A., and Turner, M. L.: Companion data to Towards global impact-based forecasting model for tropical cyclones, Google Drive [data set], http://rb.gy/f27wy (last access: 13 October 2023), 2023a.

Kooshki Forooshani, M., Turner, M., Ndirangu, P., Kaltenbrunner, A., and Teklesadik, A.: Global Tropical Storm Model, GitHub [code], https://github.com/rodekruis/GlobalTropicalCycloneModel (last access: 13 October 2023), 2023b.

Lambert, C., Landry, S., Andreu, M. G., Koeser, A., Starr, G., and Staudhammer, C.: Impact of model choice in predicting urban forest storm damage when data is uncertain, Landscape Urban Plan., 226, 104467, https://doi.org/10.1016/j.landurbplan.2022.104467, 2022.

Liu, D., Pang, L., and Xie, B.: Typhoon disaster in China: prediction, prevention, and mitigation, Nat. Hazards, 49, 421–436, 2009.

Lundberg, S. and Lee, S.-I.: A unified approach to interpreting model predictions, arXiv [preprint], arXiv:1705.07874, https://doi.org/10.48550/arXiv.1705.07874, 2017a.

Lundberg, S. M. and Lee, S.-I.: A Unified Approach to Interpreting Model Predictions, in: 31st Annual Conference on Neural Information Processing Systems (NIPS 2017), 4–9 December 2017, Long Beach, California, USA, 4765–4774, ISBN 9781510860964, 2017b.

Lundberg, S. M., Erion, G., Chen, H., DeGrave, A., Prutkin, J. M., Nair, B., Katz, R., Himmelfarb, J., Bansal, N., and Lee, S.-I.: Explainable AI for Trees: From Local Explanations to Global Understanding, arXiv [preprint], https://doi.org/10.48550/arXiv.1905.04610, 2019.

MacLeod, D., Easton-Calabria, E., de Perez, E. C., and Jaime, C.: Verification of forecasts for extreme rainfall, tropical cyclones, flood and storm surge over Myanmar and the Philippines, Weather and Climate Extremes, 33, 100325, https://doi.org/10.1016/j.wace.2021.100325, 2021.

Masinde, B., Gevaert, C., van den Homberg, M., Nagenborg, M., Gortzak, I., Margutti, J., and Zevenbergen, J.: Auditing a flood vulnerability geo-intelligence workflow for biases, submitted, 2023.

Mendelsohn, R., Emanuel, K., Chonabayashi, S., and Bakkensen, L.: The impact of climate change on global tropical cyclone damage, Nat. Clim. Change, 2, 205–209, 2012.

Navarro, A. and Merino, A.: Chapter 20 – Precipitation in Earth system models: advances and limitations, in: Precipitation Science, edited by: Michaelides, S., Elsevier, 637–659, ISBN 978-0-12-822973-6, https://doi.org/10.1016/B978-0-12-822973-6.00013-5, 2022.

PAGASA: Philippine Atmospheric, Geophysical and Astronomical Services Administration, https://www.pagasa.dost.gov.ph/ (last access: 13 October 2023), 2023.

ReliefWeb: Philippines: Anticipatory Action Framework, 2022 Revision, https://reliefweb.int/report/philippines/philippines-anticipatory-action-framework-2022-revision (last access: 13 October 2023), 2022.

Rogers, R. F., Velden, C. S., Zawislak, J., and Zhang, J. A.: Tropical Cyclones and Hurricanes: Observations, in: Reference Module in Earth Systems and Environmental Sciences, Elsevier, ISBN 978-0-12-409548-9, https://doi.org/10.1016/B978-0-12-409548-9.12065-2, 2019.

Santos, G. D. C.: 2020 tropical cyclones in the Philippines: A review, Tropical Cyclone Research and Review, 10, 191–199, 2021.

Sedhain, S., van den Homberg, M., Teklesadik, A., van Aalst, M., and Kerle, N.: Explainable Impact-Based Forecasting for Tropical Cyclones, in preparation, 2023.

Taylor, H. T., Ward, B., Willis, M., and Zaleski, W.: The saffir-simpson hurricane wind scale, Atmospheric Administration: Washington, DC, USA, https://www.nhc.noaa.gov/pdf/sshws.pdf.pre20210528 (last access: 13 October 2023), 2010.

Teklesadik, A. and van den Homberg, M.: Forecasting impacts of tropical cyclones with machine learning: A case study in the Philippines, EGU General Assembly 2022, Vienna, Austria, 23–27 May 2022, EGU22-12917, https://doi.org/10.5194/egusphere-egu22-12917, 2022.

Teklesadik, A., Turner, M., Visser, J., and van der Veen, M.: 510 typhoon-impact-based-forecasting-model, GitHub [code], https://github.com/rodekruis/Typhoon-Impact-based-forecasting-model (last access: 13 October 2023), 2023.

Tierra, M. C. M. and Bagtasa, G.: Identifying the rapid intensification of tropical cyclones using the Himawari-8 satellite and their impacts in the Philippines, Int. J. Climatol., 43, 1–16, 2023.

Van Aalst, M. K.: The impacts of climate change on the risk of natural disasters, Disasters, 30, 5–18, 2006.

van Brussel, M.: Predicting rice losses due to typhoons, The case of the Philippines, Bicol region, Master's thesis, University of Amsterdam, https://arno.uvt.nl/show.cgi?fid=149411 (last access: 13 October 2023), 2021.

van den Homberg, M., Gevaert, C., and Georgiadou, Y.: The Changing Face of Accountability in Humanitarianism: Using Artificial Intelligence for Anticipatory Action, Politics and Governance, 8, 456–467, https://doi.org/10.17645/pag.v8i4.3158, 2020.

Van Lint, S., Heijmans, I. A., and van der Veen, M.: Sense-making of the Netherlands Red Cross Priority Index model: Case typhoon Haiyan, Philippines, PhD thesis, Masters dissertation), Wageningen University, the Netherlands, https://doi.org/10.1061/(ASCE)1527-6988(2006)7:2(94), 2016.

Vickery, P. J., Skerlj, P. F., Lin, J., Twisdale, L. A., Young, M. A., and Lavelle, F. M.: HAZUS-MH Hurricane Model Methodology. II: Damage and Loss Estimation, Nat. Hazards Rev., 7, 94–103, https://doi.org/10.1061/(ASCE)1527-6988(2006)7:2(94), 2006.

Wagenaar, D., Lüdtke, S., Schröter, K., Bouwer, L. M., and Kreibich, H.: Regional and Temporal Transferability of Multivariable Flood Damage Models, Water Resour. Res., 54, 3688–3703, https://doi.org/10.1029/2017WR022233, 2018.

Wagenaar, D., Hermawan, T., van den Homberg, M. J., Aerts, J. C., Kreibich, H., de Moel, H., and Bouwer, L. M.: Improved transferability of data-driven damage models through sample selection bias correction, Risk Anal., 41, 37–55, 2021.

Walsh, Brian; Hallegatte, S.: Measuring Natural Risks in the Philippines Socioeconomic Resilience and Wellbeing Losses, Economics of Disasters and Climate Change, 4, 249–293, https://doi.org/10.1007/s41885-019-00047-x, 2020.

Warner, J. C., Armstrong, B., He, R., and Zambon, J. B.: Development of a coupled ocean–atmosphere–wave–sediment transport (COAWST) modeling system, Ocean Model., 35, 230–244, 2010.

Yonson, R., Noy, I., and Gaillard, J.: The measurement of disaster risk: An example from tropical cyclones in the Philippines, Rev. Dev. Econ., 22, 736–765, 2018.